

Calculating the Forced Response of a Mistuned Blisk via Surrogate Models

*Shiyuan DENG¹, †Jianyao YAO¹, Jianqiang XIN,² Chenxu JIANG¹, Teng LI¹, Dongyang SUN¹, Zejun WU¹

¹College of Aerospace Engineering, Chongqing University, China

²Research and Development Center, China Academy of Launch Vehicle Technology, China

*Presenting author: dsycircle@163.com

†Corresponding author: yaojianyao@cqu.edu.cn

Abstract

The forced responses of blisks are highly sensitive to inevitable random mistuning, which can cause severe damage. Considerable computational efforts are required for the sampling process to acquire the statistical vibration properties of mistuned blisks via finite element models. Therefore, efficient surrogate models are preferred. In this paper, four methods are utilized to construct the relation between random mistuning and forced response amplitudes. These four methods include polynomial chaos expansion (PCE), response surface method (RSM), Kriging interpolation and artificial neural networks (ANN). A lumped parameter model of a 24-sector blisk is used to investigate the vibration patterns. Each sector has 2 degrees-of-freedom (DOF). Mistuning is simulated by treating the stiffness of blades as independently identically distributed (i.i.d) random variables and Sobol sequence is applied for designing the sample sites. On assessing the result, mean squared error (MSE) and Kolmogorov-Smirnov test are applied to numerically determine the accuracy. Results show that PCE can yield the most accurate and stable predictions of the statistical characteristics of the forced responses; Kriging interpolation and ANN are also remarkable while RSM does not show any priority on this issue.

Keywords: mistuned blisks, forced response, polynomial chaos expansions, response surface method, Kriging interpolation, artificial neural networks

Introduction

Mistuning refers to inevitable variations of blisks and arises during the manufacturing and assembly process due to wear, maintenance, machining error, material dispersion, etc. These small deviations can lead to much larger response level than the ideal, tuned design^[1]. The severe amplification of vibration altitude may cause high cycle fatigue (HCF) and premature failure of the blades. As was estimated in 1998, about 30% of all engine maintenance costs were caused by HCF^[2]. Therefore, it is of great interest to accurately predict the adverse effect of mistuning on the vibration of blisks.

The mistuning across blades is randomly distributed^[3,4], thus we usually have to use the statistical properties of the forced responses of blisks to assess the effects of mistuning. The most commonly used method is Monte Carlo Simulation (MCS), which requires an amount of repetitive analysis and tiny deviations of parameters are needed in each process^[5]. Typically, finite element (FE) models are applied to carry out the calculation process^[3,3,6].

There have been numerous studies on the mistuned blisks using FE models. Slater pointed out that a complete FE model instead of a single sector was necessary because mistuning could break the cyclic symmetry^[7]. Petrov considered it as an optimization problem to search for the best and worst vibration pattern using an FE model^[8]. Castanier gave a complete FE model of a mistuned blisk^[11]. He discussed about some of the fundamental issues of mistuned disks, including coupling and mode localization, and proposed an algorithm to accelerate MCS. Laxalde built a multistage FE model for mistuned blisks and also confirmed the validity^[9]. More recently, accurate modeling of small manufacturing errors or geometric mistuning of blades is realized using the coordinate measurement methods^[10]. One of the most significant advantages that make FE models irreplaceable is the high accuracy. However, although computational capacity of modern computers has greatly improved, it is still challenging to carry out a large number of MCS based on full FE models. Therefore, much attention has been paid to reduced order models (ROM) for mistuned blisks, mainly including the component-mode-based methods and the system-mode-based methods^[11-14].

The lumped parameter models are one kind of ROM. They treat each sector as a spring-mass oscillator connected to the ground and coupled to neighboring sectors by linear springs. Although not capable of precisely representing the actual engineering structures, these models can capture some basic features of the mistuned blisks, such as the modal localization and vibration amplification^[15,16]. Also, the required computational efforts are far less than FE models. Therefore, they provide a good insight of the vibrational mechanism of mistuned blisks together with MCS.

Surrogate models are another popular approach for uncertainty analysis in engineering. Instead of direct operations on each individual sample, the surrogate models pursue to establish an analytical relationship between the random input and output based on the results obtained at designed sampling points, which is much easier to use, and once the model is obtained, the computational efforts for new points are negligible. Since the forced responses of mistuned blisks are highly sensitive to the random mistuning, the relationship between the response amplitude and mistuning is highly nonlinear and difficult to define, thus the application of surrogate models for mistuned analysis has not drawn much attention. In a previous study, we tried to use RSM and Kriging metamodel to obtain the response amplification factor over a frequency range, but only succeeded when 4 sectors out of 24 were mistuned. When the number of mistuned sectors increases, the accuracy and the required number of samples of the metamodels are not acceptable. Sinha applied the method of PCE to analytically compute the statistics of the forced response of a mistuned blisk assembly^[17]. But the proposed method is an intrusive one, which means that we have to modify the solver correspondingly. In practice, we prefer non-intrusive methods, which only need the input and output to construct the surrogate models.

In this paper, we will try to build the relation between the forced response amplitude and the mistuning via four surrogate models, namely the polynomial chaos expansions (PCE), the response surface method (RSM), the Kriging interpolation and the artificial neural network (ANN), and compare their validities. A lumped parameter model is used to generate the training data. In later parts, we will introduce: 1) The basic theories and implementations in mistuned blisks of the aforementioned four methods; 2) A numerical example of lumped parameter blisk model; 3) The validation of the four methods, followed by the results and discussions; 4) Some conclusions.

Briefs of Response Surface Method, Artificial Neural Networks, Kriging Interpolation and Polynomial Chaos Expansion

Surrogate Models for Forced Vibration Analysis of Mistuned Blisks

For a blisk, the amplitude of sector i can be denoted as A_i . If only the stiffness mistuning is considered, A_i is determined by system stiffness matrix \mathbf{K} , which consists of stiffness of the sectors:

$$A_i = A_i(\mathbf{K}) \quad (1)$$

If we have n random variables $\mathbf{v} = [v_1, v_2, \dots, v_n]^T$ representing the input random mistuning for n sectors, and the scalar output $u(f_j)$, which is the amplitude of forced response with excitation frequency f_j , the target surrogate model can be written as

$$u(f_j) \approx f(\mathbf{v}) \quad (2)$$

In this paper, f refers to PCE, RSM, Kriging interpolation and ANN and can be obtained using the designed training points, which will be described in the following subsections.

We use the cross validation method to verify the surrogate models. Typically, the sample set is partitioned into two parts. One part is called the training set, noted as D , used to build a model, and the other is called the test set, noted as T , used to verify the model. Generally, D and T are guaranteed to be i.i.d. The sample sizes are respectively written as $|D|$ and $|T|$. Error on T will be a significant indicator of the model validity. If the accuracy of the constructed surrogate model is acceptable, we can use it for the response analysis with other random mistuning to obtain the statistical characteristics. If not, we need to update or add some new training points to create a new model and validate it again. The implementation procedure is illustrated in figure 1.

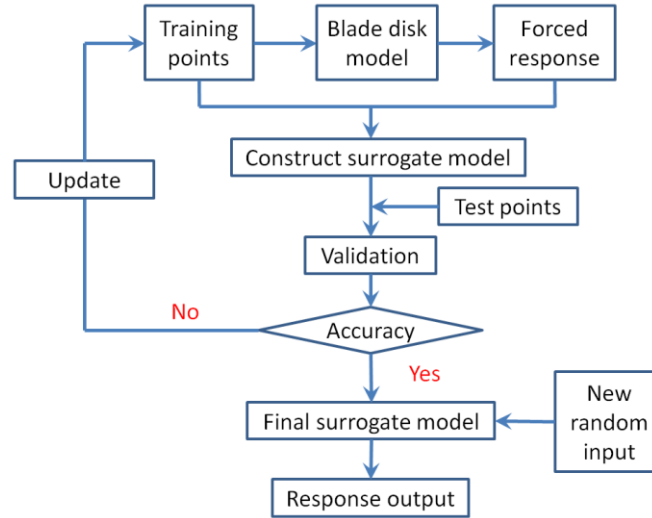


Figure 1. The flowchart for establishing the surrogate models for forced response analysis of mistuned blisks

Polynomial Chaos Expansion

The method of PCE expands the stochastic process $u = u(\mathbf{v})$ into an infinite series^[18]:

$$u = u(\mathbf{v}) = \sum_{k=0}^{\infty} \alpha_k \phi_k(\mathbf{v}) \quad (3)$$

where $\phi_k(\cdot)$ is a polynomial basis and α_k is the corresponding coefficient. Often this expression is truncated to m terms as an approximation of the infinite orthogonal series:

$$\sum_{k=0}^{\infty} \alpha_k \phi_k(\mathbf{v}) \approx \sum_{k=1}^m \alpha_k \phi_k(\mathbf{v}) \quad (4)$$

Apparently, the key to validate Eq. (4) is determine the coefficients α_k 's.

Generally, the number of terms, m , is governed by n^r , where r refers to the order of polynomial basis that are included. In other words, there is an exponential growth in m as r gets large, making high order PCE inappropriate. Second-order PCE is used later in this paper.

In addition, orthogonality of the polynomials has to be guaranteed, namely the inner product of ϕ_k and ϕ_l is always equal to 0 when $k \neq l$:

$$\langle \phi_k, \phi_l \rangle = \int_{-\infty}^{\infty} \phi_k(\mathbf{v}) \phi_l(\mathbf{v}) p(\mathbf{v}) d\mathbf{v} = 0 \quad (5)$$

where $p(\mathbf{v})$ is the weight function, generally substituted by the probability density function (PDF) of \mathbf{v} . Make an inner product of u and ϕ_l and one can obtain

$$\langle u, \phi_k \rangle = \alpha_k \langle \phi_k, \phi_k \rangle \quad (6)$$

due to the orthogonality.

Therefore, to compute the coefficients α_k , we only need to divide $\langle u, \phi_k \rangle$ by $\langle \phi_k, \phi_k \rangle$:

$$\alpha_k = \frac{\langle u, \phi_k \rangle}{\langle \phi_k, \phi_k \rangle} = \frac{\int_{-\infty}^{\infty} u(\mathbf{v}) \phi_k(\mathbf{v}) p(\mathbf{v}) d\mathbf{v}}{\int_{-\infty}^{\infty} \phi_k^2(\mathbf{v}) p(\mathbf{v}) d\mathbf{v}} \quad (7)$$

Now that we have the coefficients, numerical integral schemes are often applied to obtain the upper part of Eq. (7). On designing the integral sites of $u(\mathbf{v})$, we use Sobol sequence to accomplish the above integral.

Response Surface Method

RSM is a traditional but quite widely-used method. The main idea is to use a sequence of designed experiments to obtain an optimal response. Box and Wilson acknowledge that this model is only an approximation, but such a model is easy to estimate and apply, even when little is known about the process^[19,20]. RSM is actually an extension of least square regression. It treats $u(\mathbf{v})$ as a linear combination of first and second order terms of \mathbf{v} :

$$u(\mathbf{v}) \approx f(\mathbf{v}) = \boldsymbol{\beta}^T \tilde{\mathbf{v}} = \beta_0 + \sum_{i=1}^n \beta_i v_i + \sum_{j=1}^n \sum_{i=1}^n \beta_{ij} v_i v_j \quad (8)$$

where $\tilde{\mathbf{v}} = [1, v_1, \dots, v_n, v_1^2, v_1 v_2, \dots, v_n^2]^T$ is the augmentation of \mathbf{v} , and $\boldsymbol{\beta} = [\beta_0, \beta_1, \dots, \beta_{nn}]^T$ is the coefficient vector. If we note matrices \mathbf{V} and \mathbf{F} as the samples from D :

$$\mathbf{V} = [\tilde{\mathbf{v}}_1, \tilde{\mathbf{v}}_2, \dots, \tilde{\mathbf{v}}_d] = \begin{bmatrix} 1 & 1 & \dots & 1 \\ v_{11} & v_{12} & \dots & v_{1d} \\ \vdots & \vdots & \ddots & \vdots \\ v_{n1}^2 & v_{n2}^2 & \dots & v_{nd}^2 \end{bmatrix}, \mathbf{F} = [f(\mathbf{v}_1), f(\mathbf{v}_2), \dots, f(\mathbf{v}_d)]$$

Then we have

$$\mathbf{F} = \boldsymbol{\beta}^T \mathbf{V} \quad (9)$$

and the least square estimation of $\boldsymbol{\beta}$ is

$$\hat{\boldsymbol{\beta}} = (\mathbf{V}\mathbf{V}^T)^{-1} \mathbf{V}\mathbf{F}^T \quad (10)$$

Kriging Model

Kriging interpolation can be expressed as a two-step process: first, the covariance structure of the samples in D is determined by fitting a variogram; second, weights derived from this covariance structure are used to interpolate values for samples in T . The Kriging model can be considered as a parametric model combined with a random process which simulates the prediction error, denoted as Eq. (11):

$$u(\mathbf{v}) = f(\boldsymbol{\beta}, \mathbf{v}) + \epsilon(\mathbf{v}) \quad (11)$$

where $f(\boldsymbol{\beta}, \mathbf{v})$ is a combination of several basis functions; $\boldsymbol{\beta}$ is a vector containing the parameters in need; $\epsilon(\mathbf{v})$ is used to model the error. $\epsilon(\mathbf{v})$ satisfies the following properties:

$$\begin{aligned} E[\epsilon(\mathbf{v})] &= 0 \\ \text{Var}[\epsilon(\mathbf{v})] &= \sigma^2 \\ \text{Cov}[\epsilon(\mathbf{v}^{(i)}), \epsilon(\mathbf{v}^{(j)})] &= \sigma^2 R(\mathbf{v}^{(i)}, \mathbf{v}^{(j)}) \end{aligned} \quad (12)$$

The matrix $R(\mathbf{v}^{(i)}, \mathbf{v}^{(j)})$ is a correlation function which evaluates how close $\mathbf{v}^{(i)}$ and $\mathbf{v}^{(j)}$ are to each other. And this function is:

- 1) always positive but no larger than 1;
- 2) negative correlated to the distance between $\mathbf{v}^{(i)}$ and $\mathbf{v}^{(j)}$;
- 3) equal to 1 if and only if $\mathbf{v}^{(i)} = \mathbf{v}^{(j)}$.

In a nutshell, Kriging interpolation predicts a desired point by summing all the acquired samples based on different weights. One can infer to ^[21] for more detailed derivation.

Artificial Neural Networks

The method of artificial neural networks (ANN) was first invented in the 1940s, as an attempt to simulate the network of neurons that made up a human brain, and has been one of the main tools used in machine learning in recent years. A typical feed-forward ANN uses multiple layers of mathematical processing to make sense of the information it is fed, as is shown in Fig. 2. Here we omit the derivation and just come up with the essence that we only have to care about the input and the output and leave the calculation.

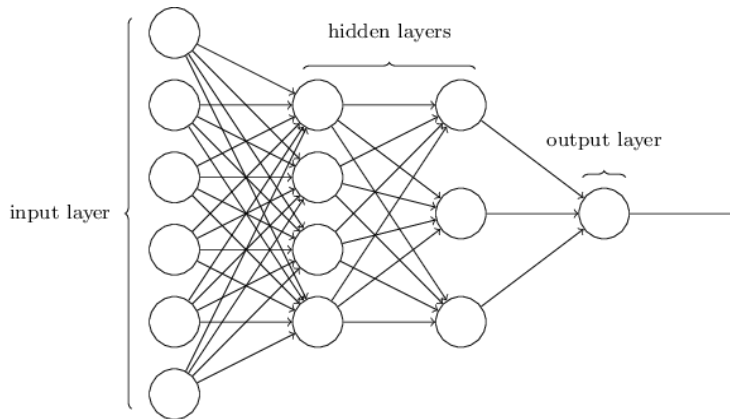


Figure 2. An example of a 4-layer feed-forward ANN

The first layer on the left in figure 2 is the input layer, which accepts the input that is fed. The first layer on the right gives the output. And the layers between, which are called hidden layers, accomplish the calculating process. In this manner, a model $u \approx f(\mathbf{v})$ is established, where u , obviously, implies the output layer and \mathbf{v} the input layer.

Typically, it plays an important role to design the structure of an ANN and to adjust parameters. In this paper, we make use of ‘Sci-Kit Learn ¹’, a scientific computation package for Python to accomplish the construction, and we only focus on the performance of ANN when applied to the analysis of mistuned blisks.

Numerical Example of a Mistuned Blisk

Lumped Parameter Model

The lumped parameter model of the blisk is illustrated in figure 3 with a cyclic chain of spring-mass oscillators with several degrees of freedom for each sector^[22]. For each sector of the blisk, the springs are massless, x_1 and x_2 describe the vibration of blade and disk, m_1, m_2, k_1 and k_2 are the equivalent mass and stiffness of blade and disk, respectively. k_c denotes the coupling stiffness between every two sectors. c is the damping of the blade. Here, we set $n = 24, c = 0.005, f = 1, m_1 = 1, m_2 = 426, k_1 = 1, k_2 = 1.1, k_c = 493$.

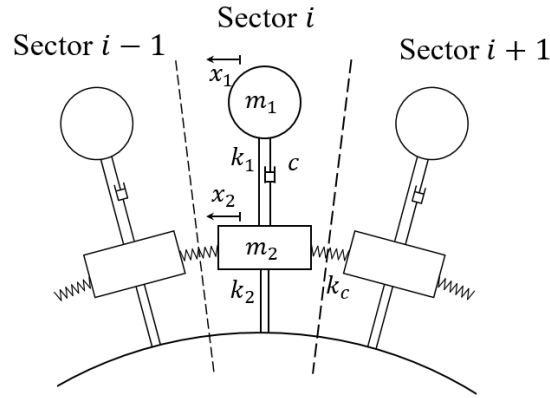


Figure 3. A lumped parameter model of a blisk

The sector stiffness matrix can be written as

$$\mathbf{K}_i = \begin{bmatrix} k_1 & -k_1 \\ -k_1 & k_1 + k_2 + 2k_c \end{bmatrix}, \mathbf{K}_c = \begin{bmatrix} 0 & 0 \\ 0 & -k_c \end{bmatrix} \quad (13)$$

Therefore, for an n -sector blisk, its system stiffness matrix \mathbf{K} , mass matrix \mathbf{M} and damping matrix \mathbf{C} can be denoted as:

$$\mathbf{K} = \begin{bmatrix} \mathbf{K}_1 & \mathbf{K}_c & 0 & \cdots & \mathbf{K}_c \\ \mathbf{K}_c & \mathbf{K}_2 & \mathbf{K}_c & \cdots & 0 \\ 0 & \mathbf{K}_c & \mathbf{K}_3 & \cdots & 0 \\ \vdots & \vdots & \vdots & \ddots & \vdots \\ \mathbf{K}_c & 0 & 0 & \cdots & \mathbf{K}_n \end{bmatrix}, \mathbf{M} = \begin{bmatrix} \mathbf{M}_1 & 0 & \cdots & 0 \\ 0 & \mathbf{M}_2 & \cdots & 0 \\ \vdots & \vdots & \ddots & \vdots \\ 0 & 0 & \cdots & \mathbf{M}_n \end{bmatrix}, \mathbf{C} = \begin{bmatrix} \mathbf{C}_1 & 0 & \cdots & 0 \\ 0 & \mathbf{C}_2 & \cdots & 0 \\ \vdots & \vdots & \ddots & \vdots \\ 0 & 0 & \cdots & \mathbf{C}_n \end{bmatrix}$$

where

$$\mathbf{M}_i = \begin{bmatrix} m_1 & 0 \\ 0 & m_2 \end{bmatrix}, \mathbf{C}_i = \begin{bmatrix} c & 0 \\ 0 & 0 \end{bmatrix}, i = 1, 2, \dots, n$$

The equations of motion of the blisk can be written as

$$\mathbf{M}\ddot{\mathbf{x}} + \mathbf{C}\dot{\mathbf{x}} + \mathbf{K}\mathbf{x} = \mathbf{F} \quad (14)$$

¹ <https://scikit-learn.org/stable/>

in which, $\mathbf{F} = [F_1, F_2, \dots, F_n]^T$ refers to the excitation vector whose i -th component F_i excites the i -th sector. Usually, the excitation on each sector has the same amplitude with a fixed phase lag with the following form

$$F_i = f e^{j\psi_i} e^{j\omega t} \quad (15)$$

where $j = \sqrt{-1}$ is the imaginary unit, f is the excitation force acting on the i -th sector, ω is the excitation frequency and

$$\psi_i = \frac{2i\pi E}{n}$$

describes the blade's relative angle where $E = 4$ is the engine order.

The forced response of the blisk can be written as

$$\mathbf{A} = \mathbf{H}^{-1} \mathbf{f} \quad (16)$$

where

$$\begin{aligned} \mathbf{H} &= -\omega^2 \mathbf{M} + j\omega \mathbf{C} + \mathbf{K} \\ \mathbf{A} &= [A_1, A_2, \dots, A_{2n}]^T \\ \mathbf{f} &= f [e^{j\psi_1}, e^{j\psi_2}, \dots, e^{j\psi_{2n}}]^T \end{aligned} \quad (17)$$

We carried out a simple analysis of the vibration amplitudes. A tuned blisk with 24 sectors was investigated to capture the basic rules of excitation-response relations. Then we substituted the frequencies back in Eq. (21) to calculate the resonance amplitudes, shown in figure 4.

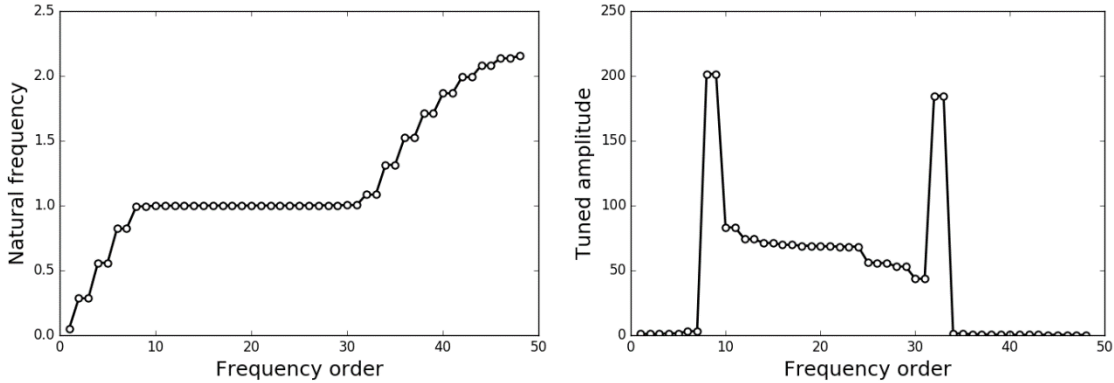


Figure 4. Natural frequencies and resonance amplitudes of the blisk

As is shown in figure 4, the largest amplitude is 201.3505, and appears when excitation frequency is 0.993. Therefore, we will set a frequency sweep near 0.993 in later sections in order to concentrate on the resonance performance of the blisk.

Stiffness Mistuning

One can simulate mistuning via a couple of methods, of which the simplest and most common one is to choose a different equivalent stiffness for every blade^[16]. This method is widely applied in relative works because deviations among blades don't change the vibration modes.

Let δ_i be the relative variation on equivalent stiffness k_1 of the i -th blade and we can use

$$k_1^i = k_1 (1 + \delta_i) \quad (18)$$

to represent the stiffness. For convenience, we write Eq. (18) as

$$k_i = k(1 + \delta_i) \quad (19)$$

Generally, we assume that δ_i 's are normally i.i.d, namely

$$\delta_i \sim N(\mu, \sigma^2), i = 1, 2, \dots, 24$$

In this paper, $\mu = 0$ and $\sigma = 0.03$.

We've known that the response amplitudes vector \mathbf{A} is influenced by the stiffness matrix \mathbf{K} , controlled by the equivalent stiffnesses k_i 's. So \mathbf{A} can be seen as a stochastic process governed by $k_1 \sim k_{24}$:

$$\mathbf{A} = A(k_1, k_2, \dots, k_{24}) \quad (20)$$

In the following section, we will illustrate the results of the four surrogate models, and make a comparison.

Results and Discussions

In this section, we will build the four surrogate models based on sample set D and testify the results on T which contains 1000 samples.

Two issues will be considered:

- 1) to investigate the relation between $|D|$ and the prediction accuracy;
- 2) to investigate the forced responses under 5 excitation frequencies near 0.993.

In terms of evaluating the error, we care about the mean squared error (MSE) and K-S test result, which is used to assess the similarity of two probability distributions.

Relation Between Sample Size and Accuracy

It is commonly acknowledged that sample size $|D|$ has a profound impact on the prediction performance of models. So firstly we want to explore the relationship between prediction accuracy and $|D|$.

Setting the excitation frequency to be $\omega = 0.993$, we examine the performance of the four methods when $|D| = 50, 100, 200$ and 500 respectively.

Figure 5 shows the relative errors comparing the four methods with MCS results under different sample sizes. Basically, PCE generates the best result, followed by Kriging interpolation and ANN. RSM is barely of use when $|D| < 500$. The relative error of PCE and RSM prediction, as one can see, shrinks dramatically when $|D|$ increases, meaning that simply adding training samples can lead to remarkable performance promotion. The result of RSM is hardly credible when D contains less samples. On the other hand, Kriging interpolation and ANN have similar results. And these two methods perform an independence on the sample size, namely, increase of $|D|$ hardly improves the performance. Further more, the prediction histograms of the four methods based on different sample sizes are plotted in figures 6 to 9.

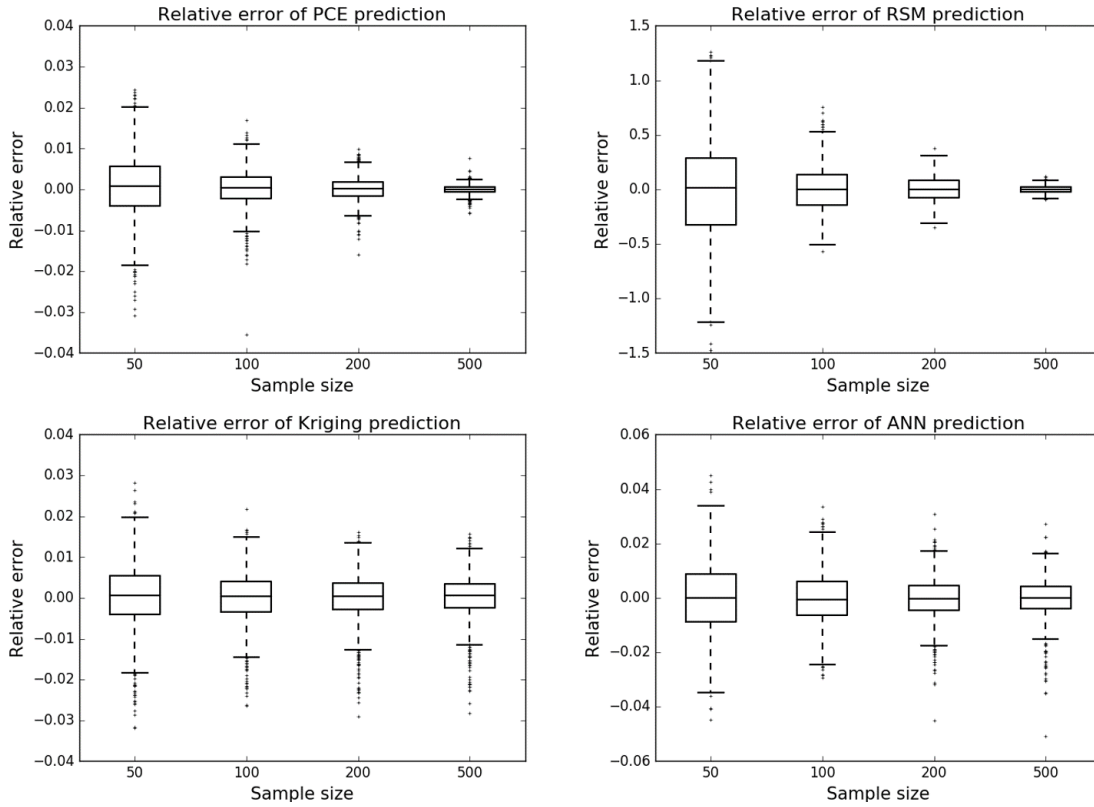


Figure 5. Boxplots of relative errors of the four methods under different sample sizes

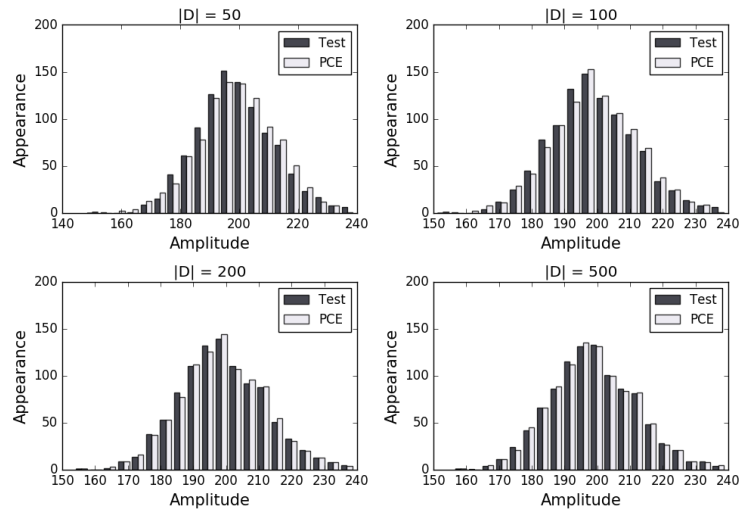


Figure 6. Histograms of PCE prediction based on four sample sizes

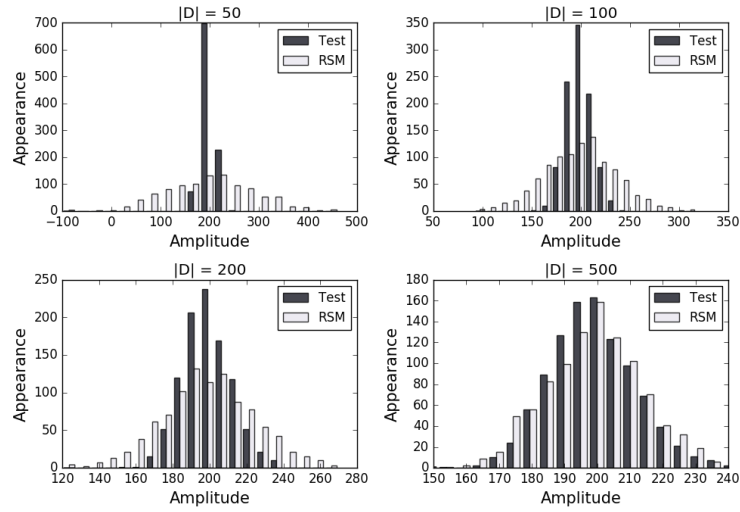


Figure 7. Histograms of RSM prediction based on four sample sizes

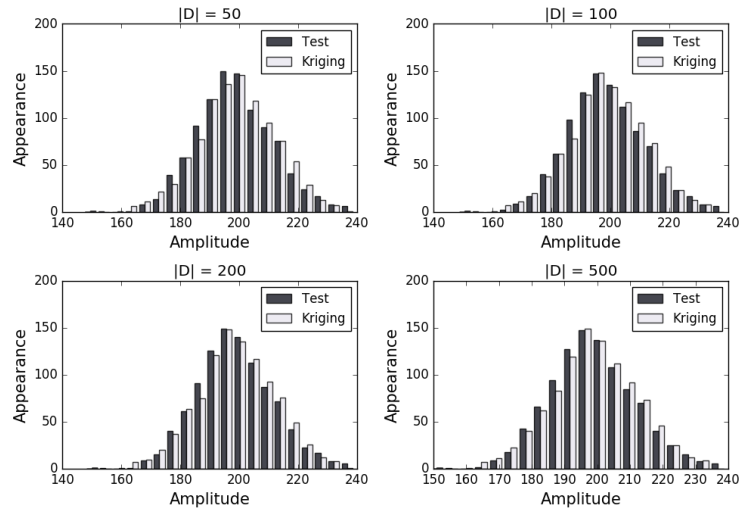


Figure 8. Histograms of Kriging prediction based on four sample sizes

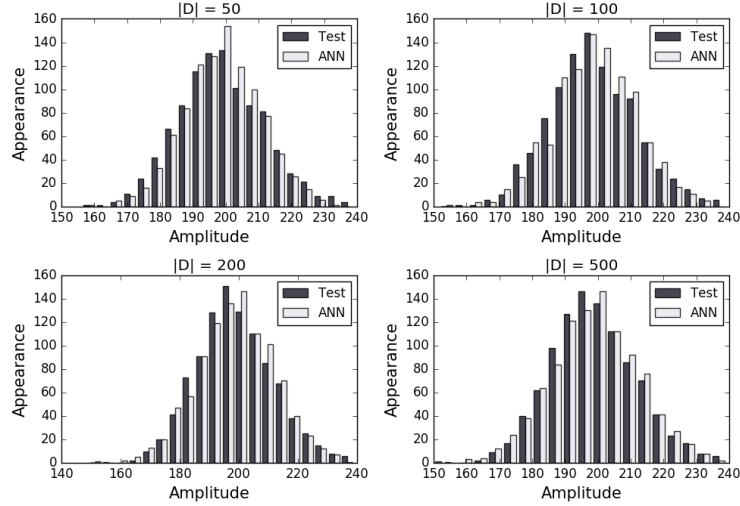


Figure 9. Histograms of ANN prediction based on four sample sizes. One can clearly see that the distribution of PCE prediction matches best with that of MCS result. When $|D| \geq 200$, the data sets look almost identical. So we will use a training set with $|D| = 200$ in later parts. Although there seems to be apparent differences in the middle parts, PCE predictions always perform well in the tail parts, namely extreme values. And extreme values should draw more attention because they are more likely to cause failure. On the other hand, Kriging interpolation and ANN also perform quite good utility. RSM hardly captures the essence of the distribution when $|D| \leq 500$.

Moreover, MSE and K-S test result of the four methods are listed in table 1, where KST represents the result of K-S test.

Table 1. Similarity of predictions and samples with different sample sizes

Sample size	PCE		RSM		Kriging		ANN	
	MSE	KST	MSE	KST	MSE	KST	MSE	KST
50	6.30e-4	0.95	0.21	0.00	8.12e-4	0.68	9.62e-4	0.00
100	3.55e-4	0.91	4.36e-2	0.00	5.96e-4	0.91	1.19e-3	0.46
200	1.04e-4	0.99	1.38e-2	0.00	5.09e-4	0.98	1.54e-3	0.08
500	2.87e-5	0.99	1.43e-3	0.34	4.53e-4	0.88	7.89e-4	0.31

Prediction under Different Frequencies

Next, we set a frequency sweep: $\omega = 0.991, 0.992, 0.993, 0.994$ and 0.995 , trying to figure out to which frequency the blades resonate the most and whether the four methods work when $|D| = 200$. The error boxplots and the histograms are shown in figures 10 to 13, and specific statistical results are listed in table 2.

The result of PCE is shown in figure 10, containing the relative error and the histograms paired with that of MCS. Apparently, the accuracy of PCE is sufficiently guaranteed.

Figure 11 shows the prediction of RS. One can clearly see that the result is much worse than that of PCE predictions. And RSM gives some predictions that differ from test samples by over 30%, which are hard to be treated as valid results. Moreover, we can see from the histograms that RSM captures the mean values well, but it fails to predict the flank parts.

One can see from figure 12 that Kriging prediction histograms resemble those of test samples well, a little worse than PCE but far better than RSM and ANN.

In this paper, a one-hidden-layer ANN is used. The number of neurons in hidden layer is 20; activation function is radial basis function (RBF); solver algorithm is gradient descent; step size is 0.0001 and max iteration number is 1000. Above work is done in Python, “scikit-learn” package specifically. The result is shown in figure 13.

As is shown in the histograms of figure 13, ANN can yield sufficiently accurate result. In a word, this method has a promising convergence comparing to RSM when its model parameters are appropriately chosen, which often needs manual intervention, making it not as good as PCE and Kriging interpolation.

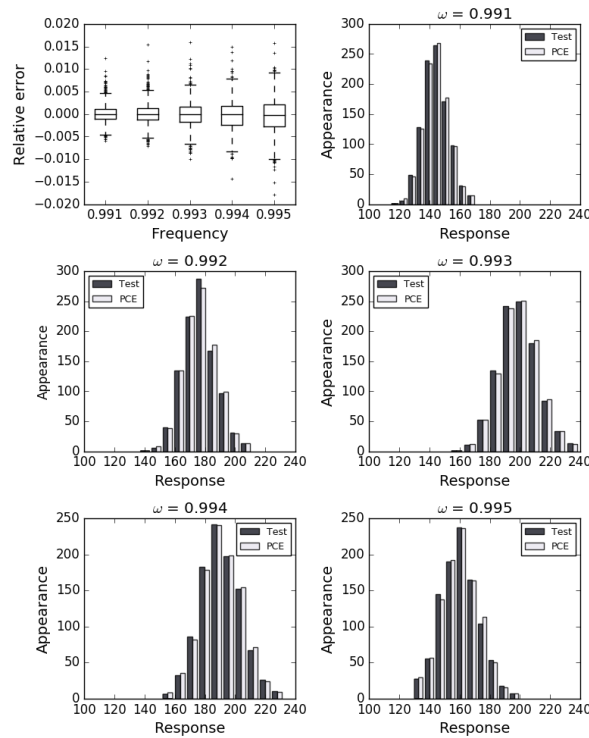


Figure 10. PCE predictions under different excitation frequencies based on 200 samples

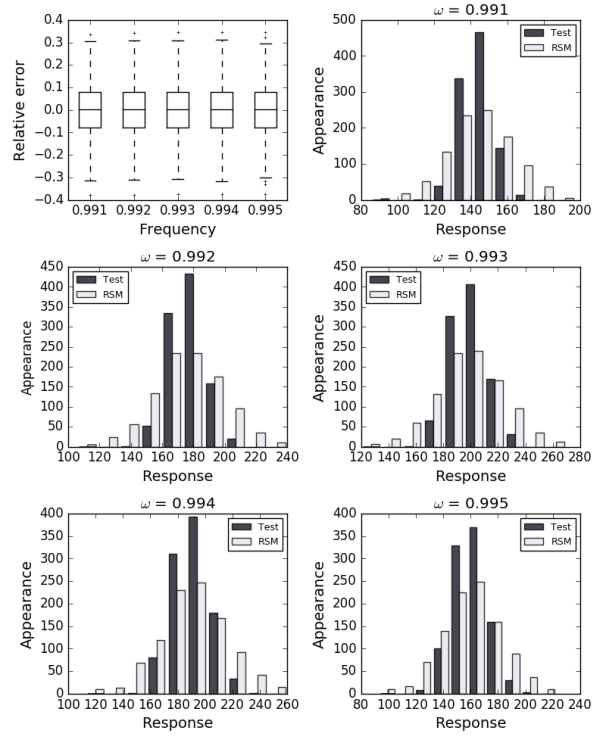


Figure 11. RSM predictions under different excitation frequencies

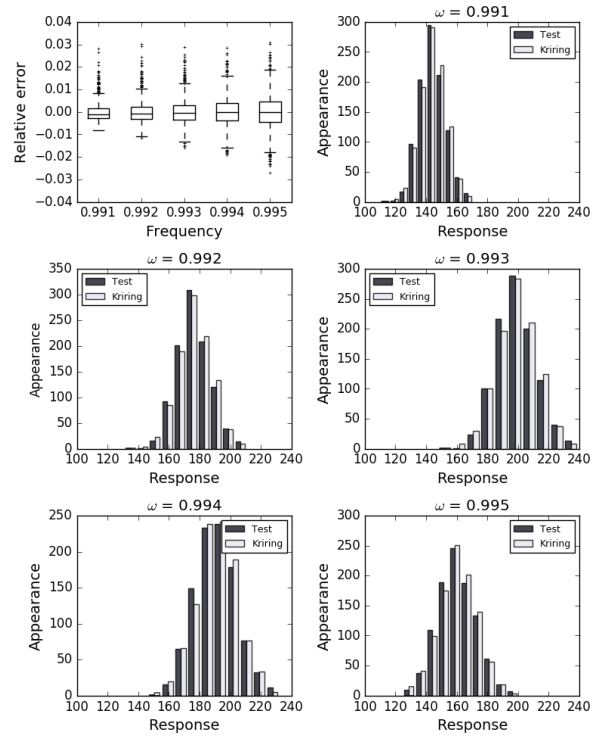


Figure 12. Kriging predictions under different excitation frequencies

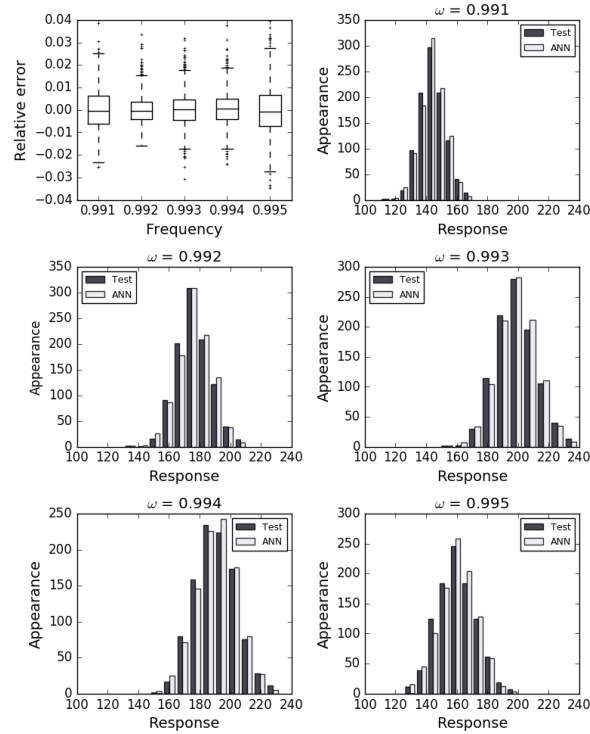


Figure 13. ANN predictions under different excitation frequencies

Table 2. Similarity of predictions and samples under different excitation frequencies

Freq.	PCE		RSM		Kriging		ANN	
	MSE	KST	MSE	KST	MSE	KST	MSE	KST
0.998	6.25e-5	0.99	1.31e-2	0.00	1.13e-4	0.98	9.62e-4	0.08
0.999	1.07e-4	0.99	1.33e-2	0.00	3.39e-4	0.88	2.77e-3	0.60
1.000	1.04e-4	0.99	1.38e-2	0.00	5.09e-4	0.98	1.54e-3	0.61
1.001	9.62e-5	0.98	1.38e-2	0.00	3.36e-4	0.72	4.21e-3	0.00
1.002	5.59e-5	0.98	1.36e-2	0.88	1.31e-4	0.99	5.73e-3	0.00

Obviously, PCE provides the most valid and stable results, because MSE and KST of PCE are both the best among the four methods. And the distribution best resembles that of test set. Kriging interpolation and ANN are also remarkable on this issue. RSM fails to model the vibration properly, making it hard to be of actual use.

Conclusion

The statistics of forced response of a mistuned blisk have been calculated via second-order PCE and three other methods. mean square error in addition with the K-S test result of predictions of the four methods have been computed and discussed. With 200 training samples, PCE can yield the most accurate and convergent result, followed by Kriging interpolation and ANN. RSM seems to be inappropriate on this issue. The accuracy of PCE and RSM increases when the sample size gets large. In addition, PCE provides a functional relationship between mistuning variables and the response amplitudes, which can be used

for further analysis on the sensitivity of amplitudes to the variables for numerical optimization.

The analysis and results presented in this paper can be easily applied to lumped-parameter models even with more degrees of freedom in future works. Only the k_1^i 's will have to be redefined.

References

- [1] CASTANIER M P, PIERRE C. Modeling and analysis of mistuned bladed disk vibration: status and emerging directions. *Journal of Propulsion and Power*, 2006, 22(2): 384–396.
- [2] THOMSON D E, GRIFFIN J T. The national turbine engine high cycle fatigue program. *Global Gas Turbine News*, 1999, 39(1): 14–17.
- [3] DYE R, HENRY T. Vibration amplitudes of compressor blades resulting from scatter in blade natural frequencies. *Journal of Engineering for Power*, 1969, 91(3): 182–187.
- [4] KAZA K R V, KIELB R E. Vibration and flutter of mistuned bladed-disk assemblies. *Journal of Propulsion and Power*, 1985, 1(5): 336–344.
- [5] GRIFFIN J, HOOSAC T. Model development and statistical investigation of turbine blade mistuning. *Journal of Vibration, Acoustics, Stress, and Reliability in Design*, 1984, 106(2): 204–210.
- [6] EWINS D. Vibration characteristics of bladed disc assemblies. *Journal of Mechanical Engineering Science*, 1973, 15(3): 165–186.
- [7] SLATER J, MINKIEWICZ G, BLAIR A. Forced response of bladed disk assemblies—a survey. *34th AIAA/ASME/SAE/ASEE Joint Propulsion Conference and Exhibit*. 1999: 3743.
- [8] PETROV E P. Explicit finite element models of friction dampers in forced response analysis of bladed disks. *Journal of engineering for gas turbines and power*, 2008, 130(2): 022502.
- [9] LAXALDE D, LOMBARD J-P, THOUVEREZ F. Dynamics of multistage bladed disks systems. *Journal of Engineering for Gas Turbines and Power*, 2007, 129(4): 1058–1064.
- [10] KASZYNSKI A A, BECK J A, BROWN J M. Uncertainties of an automated optical 3d geometry measurement, modeling, and analysis process for mistuned integrally bladed rotor reverse engineering. *Journal of Engineering for Gas Turbines and Power*, 2013, 135(10): 102504.
- [11] CASTANIER M P, OTTARSSON G, PIERRE C. A reduced order modeling technique for mistuned bladed disks. *Journal of Vibration and Acoustics*, 1997, 119(3): 439–447.
- [12] LIM S-H, BLADH R, CASTANIER M P et al. Compact, generalized component mode mistuning representation for modeling bladed disk vibration. *AIAA journal*, 2007, 45(9): 2285–2298.
- [13] VARGIU P, FIRRONE C M, ZUCCA S et al. A reduced order model based on sector mistuning for the dynamic analysis of mistuned bladed disks. *International Journal of Mechanical Sciences*, 2011, 53(8): 639–646.
- [14] ELHAMI A, LALLEMENT G, MINOTTI P et al. Methods that combine finite group theory with component mode synthesis in the analysis of repetitive structures. *Computers & structures*, 1993, 48(6): 975–982.
- [15] CHEN S, SINHA A. Calculating the statistics of the maximum amplitude of a mistuned bladed disk assembly. *33rd Structures, Structural Dynamics and Materials Conference*. 1992: 2217.
- [16] SINHA A. Computation of the Statistics of Forced Response of a Mistuned Bladed Disk Assembly via Polynomial Chaos. *Journal of Vibration and Acoustics*, 2006, 128(4): 449.
- [17] SINHA A. Calculating the statistics of forced response of a mistuned bladed disk assembly. *AIAA journal*, 1986, 24(11): 1797–1801.
- [18] THAPA M, MULANI S B, WALTERS R W. A new non-intrusive polynomial chaos using higher order sensitivities. *Computer Methods in Applied Mechanics and Engineering*, 2018, 328: 594–611.
- [19] BOX G, WILSON K. On the Experimental Attainment of Optimum Conditions. *Journal of the Royal Statistical Society. Series B (Methodological)*, 1951, 13(1): 1–45.
- [20] JONES D R, SCHONLAU M, WELCH W J. Efficient global optimization of expensive black-box functions. *Journal of Global optimization*, 1998, 13(4): 455–492.
- [21] CRESSIE N. The origins of kriging. *Mathematical geology*, 1990, 22(3): 239–252.
- [22] YAO J, WANG J, LI Q. Improved modal localization and excitation factors for understanding mistuned bladed disk response. *Journal of Propulsion and Power*, 2011, 27(1): 50–60.